` Attractor Landscape Analysis Reveals Feedback Loops in the p53 Network That Control the Cellular Response to DNA Damage

Minsoo Choi, Jue Shi, Sung Hoon Jung, Xi Chen and Kwang-Hyun Cho (20 November 2012)

Science Signaling **5** (251), ra83. [DOI: 10.1126/scisignal.2003363]

COMPUTATIONAL BIOLOGY

Attractor Landscape Analysis Reveals Feedback Loops in the p53 Network That Control the Cellular Response to DNA Damage

Minsoo Choi,[1]* Jue Shi,[2]* Sung Hoon Jung,[1,3] Xi Chen,[2] Kwang-Hyun Cho[1]†

The protein p53 functions as a tumor suppressor and can trigger either cell cycle arrest or apoptosis in response to DNA damage. We used Boolean network modeling and attractor landscape analysis to analyze the state transition dynamics of a simplified p53 network for which particular combinations of activation states of the molecules corresponded to specific cellular outcomes. Our results identified five critical interactions in the network that determined the cellular response to DNA damage, and simulations lacking any of these interactions produced states associated with sustained p53 activity, which corresponded to a cell death response. Attractor landscape analysis of the cellular response to DNA damage of the breast cancer cell line MCF7 and the effect of the Mdm2 (murine double minute 2) inhibitor nutlin-3 indicated that nutlin-3 would exhibit limited efficacy in triggering cell death, because the cell death state was not induced to a large extent by simulations with nutlin-3 and instead produced a state consistent with oscillatory p53 dynamics and cell cycle arrest. Attractor landscape analysis also suggested that combining nutlin-3 with inhibition of Wip1 would synergize to stimulate a sustained increase in p53 activity and promote p53-mediated cell death. We validated this synergistic effect in stimulating p53 activity and triggering cell death with single-cell imaging of a fluorescent p53 reporter in MCF7 cells. Thus, attractor landscape analysis of p53 network dynamics and its regulation can identify potential therapeutic strategies for treating cancer.

INTRODUCTION

Mammalian cells have evolved an efficient internal self-defense system to cope with various stresses such as DNA damage and aberrant signals that can result in oncogenesis (*1*). One critical response in the stress defense process is activation of the tumor suppressor protein p53, the central player of a stress response network. Under unstressed conditions, the amount of p53 is maintained low by Mdm2 (murine double minute 2), the E3 ubiquitin ligase that targets p53 for proteasome-mediated degradation. In response to various stress stimuli, the abundance of p53 increases and subsequently activates different stress response programs, including DNA damage repair, cell cycle arrest, senescence, or cell death by apoptosis (*2*–*4*), which can be considered different cell fates (final steady states). Single-cell analysis that focused on the p53-Mdm2 negative feedback loop in the DNA damage response revealed a dynamic pattern of p53 activity, which consisted of a series of p53 pulses that were independent of the amount of DNA damage, suggesting that the behavior of the p53 feedback loop can be thought of as "digital" (on or off) as opposed to "analog" (graded according to the intensity of the stimulus) (*4*–*6*).

Although many experimental and theoretical studies of various p53-mediated, stress response processes have been done, many questions remain because of the complexity of the p53 regulatory network (*6*–*11*). For instance, the mechanisms by which p53 controls alternative cell fate (cell cycle arrest versus cell death) under different conditions are poorly understood (*12*). Both positive and negative feedback loops contribute to the tight regulation of p53 activity and p53-modulated network dynamics, and the subsequent cellular outcomes are tightly controlled at multiple levels (*13*). To understand how the p53 network controls cell fate, it is important not only to study the network components and their molecular interactions but also to identify essential network properties at the system level.

Previous studies have shown that complex gene regulatory networks can be effectively analyzed by considering the cellular phenotype as a high-dimensional state attractor (*14*–*16*). An attractor is a mathematical concept representing a stable steady state adopted by a dynamic system, in this case a cellular regulatory network. These studies of cellular phenotype were based on the conceptual framework of an "epigenetic landscape" proposed by Conrad H. Waddington (*17*, *18*). Under this conceptual framework, a cellular transcriptional network, composed of genes and the transcription factors that regulate expression of the genes, is mapped into an attractor landscape. Each point in this landscape represents one state of the complex network and is defined by a set of state values containing the activity states of all genes in the network. Although cellular behavior is regulated by interactions among a large number of genes and proteins in the network, a single cell can switch between distinct cell fates when the activity of the genes results in the cell reaching certain characteristic stable states known as "attractors." The area around a particular stable state is called the "basin of attraction" and is the region of states with trajectories going to the "attractor" (*14*).

We applied this state-space approach to the p53 network, in which the attractor represents a stable cellular phenotype (proliferation, cell cycle arrest, senescence, or cell death). In attractor landscape analysis, each network state is represented as a point in the cellular state space, and the network is attracted either to a fixed point called the point attractor state or to a set of points called the cyclic attractor state, both of which represent the most stable states with the lowest potential energies in the state space. Whether the attractor is of the point or cyclic type has implications for cellular outcomes in response to a stimulus, such as DNA damage. A point attractor indicates a specifically determined cellular response, such as cell

[1]Department of Bio and Brain Engineering, Korea Advanced Institute of Science and Technology (KAIST), Daejeon 305-701, Republic of Korea. [2]Center for Quantitative Systems Biology and Department of Physics, Hong Kong Baptist University, Hong Kong, China. [3]Department of Information and Communication Engineering, Hansung University, Seoul 136-792, Republic of Korea.
*These authors contributed equally to this work.
†To whom correspondence should be addressed. E-mail: ckh@kaist.ac.kr

proliferation or cell death, whereas a cyclic attractor indicates the presence of oscillating biological events, such as p53 oscillations. In a cyclic attractor, p53 continuously oscillates between an active state and an inactive state. When the network adopts a cyclic attractor, cell fate is not uniquely determined.

Here, we analyze the attractor landscape and the state transition dynamics of a simplified p53 network under various cellular conditions, using a Boolean network model constructed with integrated experimental results available in the literature. The state-space analysis of the p53 network suggested that each distinct attractor state in the attractor landscape represented a p53-modulated cell fate, such as cell cycle arrest or cell death. Our results indicated that p53 dynamics was mainly controlled by interactions between p53, Mdm2, Wip1 (wild-type p53–induced phosphatase 1), cyclin G, and the DNA damage–activated kinase ATM (ataxia telangiectasia mutated). Perturbations of these interactions altered not only p53 dynamics but also cell fate. We used state-space analysis to examine the p53-mediated DNA damage response of a breast cancer cell line, MCF7, and identified an alternative, potentially more effective therapeutic strategy for enhancing cancer cell death in response to DNA-damaging chemotherapeutics. The theoretical predictions related to how perturbations would affect p53 dynamics and cellular response were validated by single-cell imaging experiments.

RESULTS

A simplified p53 network representing this pathway in a normal cell

We defined a simplified p53 network that included 16 nodes with 160 negative and 218 positive feedbacks (Fig. 1 and table S1). This simplified network consisted of multiple p53 target genes and several crosstalk pathways, such as pathways involved in survival signaling and the cell cycle regulatory pathway involving retinoblastoma (Rb) (table S1). We applied several simplification strategies to define this p53 network. First, we mainly focused on the interlinked positive and negative feedbacks to explore how the multiple feedback structures control and regulate the p53 network dynamics and the cellular response. We excluded most of the cyclins and cyclin-dependent kinases (CDKs) that are present in the G_1-S phase. Instead, we included only cyclin E, which represented the active complex of cyclin E and CDK2, because this cyclin-CDK complex participates in p53-modulated feedback. Another simplifying strategy was that we represented sets of proteins with similar pathway functions, with single nodes denoting one representative member of the set, including cyclin E for the cyclin E–CDK2 complex and ATM for the DNA damage response components, representing the kinases CHK and CHK2 and the phosphatases CDC25 and CDC25A. We limited the cellular decision to undergo cell cycle arrest or progression to the G_1-S checkpoint and did not include the G_2 and M phase checkpoints because cell cycle arrest in response to DNA damage at the G_1-S phase is p53-dependent (*19*). To dissect the dynamic behavior of this network, we divided the network into three major modules, a cell cycle control module, a p53 feedback control module, and a cell death control module [Fig. 1 and supplementary text (section 1)].

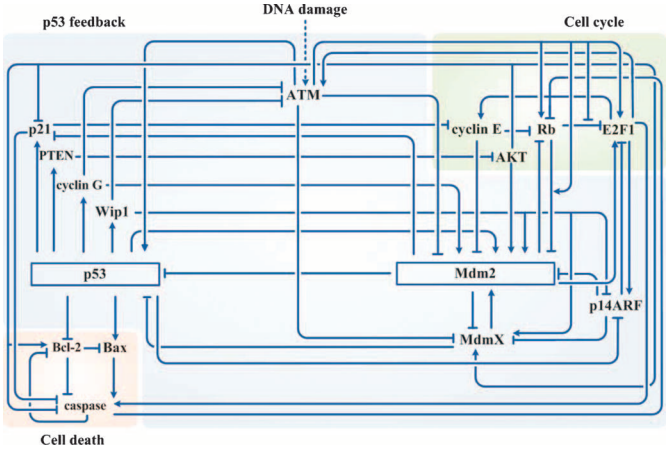

Fig. 1. Multiple feedback loops in the p53 regulatory network. There are 160 negative and 218 positive feedbacks with 50 links in the p53 regulatory network. Among them, p53 is interlinked with 136 negative and 218 positive feedbacks. Arrows indicate activating events, and perpendicular bars indicate inhibitory processes. Upon activation of ATM in response to DNA damage, activated p53 turns on interlinked positive and negative feedback loops. Among these, primary feedback regulations include the five feedback loops that target Mdm2, Wip1, cyclin G, PTEN, and p21. The light blue area represents the p53 feedback module; the light green area represents the cell cycle module; and the orange area represents the cell death module.

In the simplified p53 network in the absence of DNA damage, the abundance of p53 is low and the abundance of cyclin E (encoded by a target gene of E2F1) is high, allowing the cell cycle to progress from G_1 to S phase (*20*). Upon DNA damage, the abundance and activity of p53 increase and its dynamics are regulated by feedback loops involving p53's transcriptional targets, such as the genes encoding Mdm2, Wip1, cyclin G, the lipid and protein phosphatase PTEN, and the cell cycle inhibitor p21 (*3*, *7*, *13*, *19*, *20*). In addition, Bax (an apoptosis promoter) and Bcl-2 (an apoptosis inhibitor) are also encoded by genes regulated by p53, thus connecting p53 activity to caspase activation and cell death (*21*). The goals of our analysis were to determine whether activation of p53 by DNA damage resulted in cell cycle arrest or cell death and whether the dynamics of p53 activity contributed to the cellular outcome.

The attractor landscape of the simplified p53 network of a "normal" cell

To determine the state transition dynamics of the p53 regulatory network, we implemented an attractor landscape of the network using a deterministic Boolean model [supplementary text (section 2) and fig. S1] and then analyzed the state of the network under two different conditions: in the absence of DNA damage (the p53 inactive state) and in the presence of DNA damage (the p53 active state). This attractor landscape corresponds to the landscape of state transitions and attractors in the state space. Through this analysis, we identified all the attractors and their basins and examined the system properties related to sequential state transitions (Tables 1 to 3). We found that each attractor represented a particular cellular phenotype and that states in each attractor basin were all related to the same phenotype. We then extended the deterministic Boolean model to a probabilistic Boolean model based on Han and Wang's approach (*22*) that takes into account the uncertainties of biological systems, and calculated the potential energy landscape of the probabilistic Boolean network (supplementary text, section 3). Because the potential energy landscape corresponds to the landscape of potential energy distribution in the state space, it can only be defined for the probabilistic Boolean network. By computing the potential energy landscape, we identified the local energy minimum states and found that they corresponded to the attractors of the attractor landscape that we derived for the deterministic Boolean network. The correspondence between the potential energy landscapes and each of the attractor landscapes (figs. S1 and S2) is shown in Figs. 2 and 3.

Previous experiments demonstrating the oscillatory dynamics of p53 and Mdm2 were conducted on transformed cancer cells (*5*, *6*), in which

p53 activity and apoptotic signaling may be different from those of normal cells. To understand the dynamics and functions of the p53 network in "normal" cells, which we defined as having a wild-type protein profile with no activated oncogenes or malfunctioning tumor suppressors, we constructed the p53 network with these properties of normal cells and then performed attractor landscape analysis; the results showed that there was only one attractor in each landscape of the p53 network, both in the presence and absence of DNA damage (fig. S1, A and B). The corresponding potential energy landscape is shown in Fig. 2 (A and B). Previous studies reported that the robustness of a network to state perturbation is increased by the presence of coupled feedback loops (*23*–*25*). Thus, the presence of a single attractor in each landscape suggests that the p53 network of normal cells is quite robust and that the multiple positive and negative feedbacks of p53 regulatory network may contribute to this robustness and produce distinct cell fate under different conditions [supplementary text (section 4) and fig. S3].

With the normal cell network, we could define three distinct cell fates: cell proliferation, cell cycle arrest, and cell death (Table 1). Simulations that resulted in persistent activation of cyclin E and produced a point attractor defined the cell fate of cell proliferation; simulations that resulted in oscillatory activation of p53 and p21 and produced a cyclic attractor defined the fate of cell cycle arrest; and simulations that resulted in persistent activation of caspase and produced a point attractor defined the fate of cell death. In a normal cell in the absence of DNA damage, the point attractor represented the cell proliferation state (Fig. 2A and fig. S1A), with persistent activation of cyclin E (Table 1). Following DNA damage, the regulatory network adopted a cyclic attractor configuration consistent with a fate of cell cycle arrest, with oscillations of p53 and Mdm2, and with the activation of genes associated with cell cycle arrest, such as p21 (Fig. 2B, Table 1, and fig. S1B). The pulsing behavior of p53, as well as oscillations in the abundance of p53 target genes, is consistent with experimental observations (*4*, *5*, *26*, *27*). In summary, the point and cyclic attractors represented distinct cellular phenotypes, suggesting that p53 dynamics and cell fate may vary under different cellular conditions.

Identification of key nodes and links in the p53 network that control p53 dynamics and the cellular response to DNA damage

To elucidate essential connections and components that controlled the p53 pulsing pattern observed in response to DNA damage, we conducted single node or single link deletion in the p53 network, in which the corresponding node or link was assigned "0" in the simulations (tables S2 and S3). The p53 pulsing pattern triggered by DNA damage was primarily maintained by five critical links and two nodes (Fig. 2C, denoted in red) because deletion of any of these five links or the two nodes resulted in conversion of cyclic attractors to either point attractors with activated caspase or a mixture of point attractors with activated caspase and cyclic attractors (Tables 2 and 3).

Deletion of any of the five links (or the two nodes) could produce a point attractor in which both p53 and caspase were active, indicating cell death. The point attractor resulting from deleting one of the five links (Table 3) exhibited differences in the activity states of the molecules in the network from those observed without DNA damage (Table 1), which is consistent with the different outcomes of these conditions: proliferation in the absence of DNA damage and cell death in the presence of DNA damage in the absence of one of these links. Deletion of any other link other than the five links did not result in point attractor representing cell death (Table 3 and table S3). Four (p53-Wip1, p53–cyclin G, cyclin G–ATM, and Wip1-ATM) of the five critical links were identified to be involved in the negative feedback that regulates p53 through Wip1 (or cyclin G) and ATM, and the remaining Mdm2-p53

Table 1. Stable states of the p53 network of a normal cell in the presence or absence of DNA damage. The cellular states are cell proliferation (P), cell cycle arrest (A), and cell death (D). White or dark blue boxes represent protein state as "off" or "on," respectively. The presence or absence of DNA damage is represented by "1" or "0," respectively, in column 1.

DNA damage _condition	Type	ATM	p53	Mdm2	Mdmx	Wip1	cyclin G	PTEN	p21	AKT	cyclin E	Rb	E2F1	p14ARF	Bcl-2	Bax	caspase	Basin size (ratio)	Cell state
0_normal	Point			■					■	■		■		■				65,536 (1)	P
1_normal	Cyclic	■		■					■	■		■	■					65,536 (1)	A
		■							■	■		■	■	■					
		■	■						■	■	■		■	■					
		■	■			■	■	■	■	■	■			■					
			■		■	■	■	■			■	■		■					
				■	■	■	■	■			■	■							
				■								■							
1_normal Wip1 inhibition	Point	■	■	■			■	■	■			■			■	■		65,536 (1)	D

Table 2. Stable states of the p53 network in response to single node deletion. The table shows attractor states that include a point attractor with on-state of p53 and caspase after a single node deletion in the network. Deletion of any other nodes resulted in maintaining a similar cyclic attractor as observed for the intact network of normal cells. P, cell proliferation; A, cell cycle arrest; D, cell death.

DNA damage _node_deletion	Type	ATM	p53	Mdm2	Mdmx	Wip1	cyclin G	PTEN	p21	AKT	cyclin E	Rb	E2F1	p14ARF	Bcl-2	Bax	caspase	Basin size (ratio)	Cell state
1_Wip1	Point	■	■	■			■	■	■				■			■	■	65,536 (1)	D
1_cyclin G	Cyclic	■	■						■	■		■	■				■	59,792 (0.912)	A
		■	■			■		■	■	■		■				■			
		■	■	■	■	■		■			■	■				■			
		■		■		■		■			■	■				■	■		
		■										■					■		
	Point	■	■	■		■		■				■			■	■		5,744 (0.088)	D

Table 3. The stable states of the p53 network for single link deletion. The table shows attractor states that include a point attractor with on-state of p53 and caspase after a single link deletion in the network. The deleted links are indicated as upstream node to downstream node (for example, row 1_p53_Wip1 is the link by which p53 regulates Wip1). P, cell proliferation; A, cell cycle arrest; D, cell death.

DNA damage _link deletion	Type	ATM	p53	Mdm2	Mdmx	Wip1	cyclin G	PTEN	p21	AKT	cyclin E	Rb	E2F1	p14ARF	Bcl-2	Bax	caspase	Basin size (ratio)	Cell state
1_p53_Wip1	Point	1	1	1	0	0	1	1	1	0	0	0	1	0	0	1	1	65,536 (1)	D
1_p53_cyclin G	Cyclic	1	1	0	0	0	0	0	0	1	1	0	1	1	0	0	1	59,879 (0.9137)	A
		1	1	0	0	1	0	1	1	1	1	0	0	0	0	1	0		
		1	1	1	1	1	0	1	1	0	0	1	1	0	0	1	0		
		1	0	1	0	1	0	1	1	0	0	1	1	0	0	1	1		
		0	0	0	0	0	0	0	0	0	0	1	0	0	0	1	1		
	Point	1	1	1	0	1	0	1	1	0	0	1	0	0	0	1	1	5,657 (0.0863)	D
1_cyclin G_ATM	Cyclic	1	1	0	0	1	1	1	1	1	1	1	0	0	1	0	0	58,118 (0.8868)	A
		1	1	0	1	1	1	1	1	0	0	1	1	0	1	0	0		
		1	1	1	1	1	1	1	1	0	0	1	1	0	0	0	0		
		1	0	1	0	1	1	1	1	0	0	1	1	0	0	1	0		
		1	0	1	0	0	0	0	0	0	0	1	1	0	0	0	1		
		1	0	0	0	0	0	0	0	1	1	0	1	1	0	0	1		
		1	1	0	0	0	0	0	0	1	1	0	0	1	1	0	0		
	Point	1	1	1	0	1	1	1	1	0	0	0	1	0	0	1	1	7,418 (0.1132)	D
1_Wip1_ATM	Cyclic	1	1	0	0	1	1	1	1	1	1	1	0	0	1	0	0	58,187 (0.8879)	A
		1	1	0	1	1	1	1	1	0	0	1	1	0	1	0	0		
		1	1	1	1	1	1	1	1	0	0	1	1	0	0	0	0		
		1	0	1	0	1	1	1	1	0	0	1	1	0	0	1	0		
		1	0	1	0	0	0	0	0	0	0	1	1	0	0	0	1		
		1	0	0	0	0	0	0	0	1	1	0	1	1	0	0	1		
		1	1	0	0	0	0	0	0	1	1	0	0	1	1	0	0		
	Point	1	1	1	0	1	1	1	1	0	0	0	1	0	0	1	1	7,349 (0.1121)	D
1_Mdm2_p53	Point	0	1	1	0	1	1	1	1	0	0	0	1	0	0	1	1	65,536 (1)	D

link was involved in the negative feedback between Mdm2 and p53. The p53 network had a cyclic attractor only if both p53-Wip1 and Mdm2-p53 links were present (Table 3). Moreover, deletion of the Mdm2-p53 interaction resulted in conversion of the cyclic attractor observed in normal cells in the presence of DNA damage associated with cell cycle arrest (Table 1, 1_normal) to point attractor associated with cell death (Table 3, 1_Mdm2_p53). This suggested that the Mdm2-p53 relationship is critical to establishing a flexible cellular outcome.

The single node and single link deletion analysis suggested that p53 dynamics in response to DNA damage may assume two distinct modes: either of a series of pulses or of a sustained increase (Fig. 2D). Most previous reports have only shown pulsing p53 and suggested that cell fate is determined by the number of p53 pulses that reflect the magnitude of DNA damage (*28*). However, our results and the recent work by Purvis *et al*. (*29*) suggested that both pulsing and sustained activity of p53 are important dynamic modes of p53 activity. Conditions that produced a cyclic attractor, such as DNA damage in normal cells (Table 1, 1_normal), exhibited states when p53 was active and states when p53 was inactive, suggesting that p53 activity was pulsing. Conditions that resulted in a point attractor in response to DNA damage consistently had p53 in the active state (all conditions in which the cell fate was death in Tables 1 to 3), suggesting that p53 activity was sustained.

The two distinct p53 dynamics indicated by the presence of either a cyclic attractor or a point attractor determine whether p53 induced cell cycle arrest or cell death, respectively. It has been suggested that the dynamics of p53 activity may depend on the amount and reparability of the DNA damage (*5*). In response to reparable DNA damage, p53 is more likely to promote cell survival by activating cell cycle arrest and DNA repair. When irreparable DNA damage occurs, p53 induces cell death by apoptosis to prevent tumorigenesis (*30*). Although we defined DNA damage as either present or absent in our analysis, the resulting point attractor or cyclic attractor states produced by the node and link deletion experiments indicated that our analysis could discriminate between conditions that produced "reparable" or "irreparable" DNA damage. Our model analysis indicated that whether cell responded as though the damage was reparable or irreparable was determined by the status of the p53 network. If the cell responded as though the DNA damage was reparable, all of the red links in Fig. 2C were active, but loss of any one of those critical links resulted in the cell responding as though the DNA damage was irreparable.

Wip1 was one of the two critical nodes that controlled p53 network dynamics and the cellular response to DNA damage. Wip1 is transcriptionally activated by p53, and its negative regulator, miR-16, is also induced upon DNA damage (*31*, *32*). miR-16 specifically targets *Wip1* mRNA for degradation and thus inhibits the production of Wip1 in response to DNA damage. We propose that as the severity of DNA damage increases, the inhibition of Wip1 by miR-16 may increase, which would be the cellular equivalent of removing Wip1 node in the p53 network. Therefore, we simulated the network with Wip1 inhibited and performed attractor landscape analysis (Table 1 and fig. S1C). The model showed that Wip1 deletion produced a point attractor in which caspase was activated, indicating a cell fate of cell death (Fig. 2E and Table 2). The state produced by Wip1 inhibition (Table 1) matched that produced by Wip1 deletion (Table 2).

The attractor landscape of p53 network of the MCF7 breast cancer cell line

We extended our analysis of the p53 network to a representative breast cancer cell line, MCF7. Although MCF7 cells have wild-type p53, these cells have several prominent abnormal features distinct from normal cells: (i) PTEN abundance is low because of promoter methylation (*4*); (ii) the *p14ARF* gene is not expressed under basal conditions (*4*); (iii) the abundance of cyclin G (mRNA and protein) is high under basal conditions (*33*); and (iv) caspase 3 is not expressed (*34*).

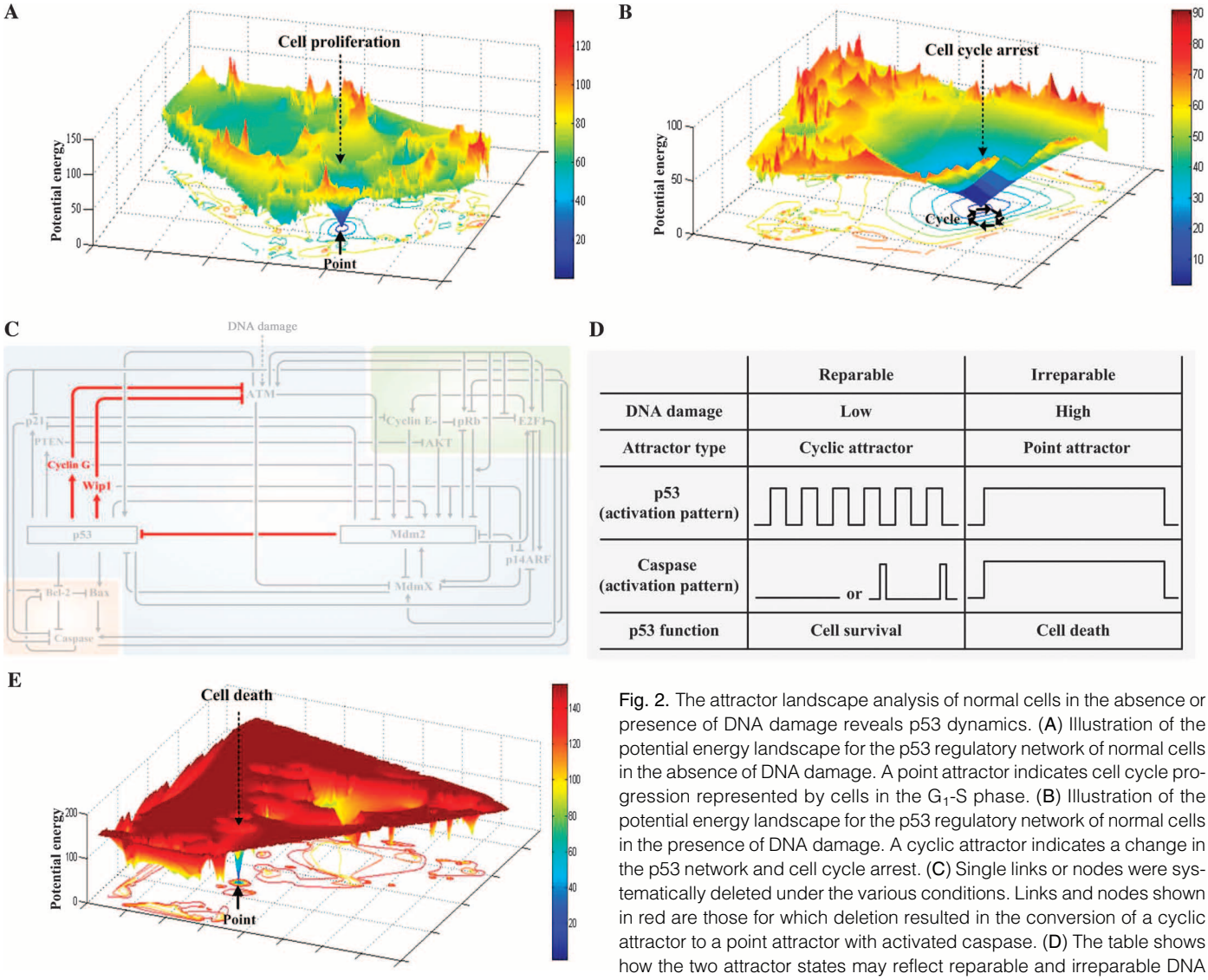

Fig. 2. The attractor landscape analysis of normal cells in the absence or presence of DNA damage reveals p53 dynamics. (**A**) Illustration of the potential energy landscape for the p53 regulatory network of normal cells in the absence of DNA damage. A point attractor indicates cell cycle progression represented by cells in the G_1-S phase. (**B**) Illustration of the potential energy landscape for the p53 regulatory network of normal cells in the presence of DNA damage. A cyclic attractor indicates a change in the p53 network and cell cycle arrest. (**C**) Single links or nodes were systematically deleted under the various conditions. Links and nodes shown in red are those for which deletion resulted in the conversion of a cyclic attractor to a point attractor with activated caspase. (**D**) The table shows how the two attractor states may reflect reparable and irreparable DNA damage. (**E**) Attractor landscape with the Wip1 node deletion. The presence of a point attractor with activated p53 and caspase (see Table 2) is indicative of cell death by apoptosis.

To reflect the abnormal gene expression in MCF7 cell in our state-space analysis, we made PTEN and p14ARF inactive ("0") and cyclin G active ("1"). The state of caspase was not fixed as inactive because the caspase node in our model included functional caspases 7, 6, and 9, in addition to the absent caspase 3. Because cyclin G, PTEN, and p14ARF activity states are restricted (preset), the potential energy landscape was relatively flat for the p53 network of MCF7 cells (Fig. 3, A and B) as compared to that of the normal cells, which contains numerous peaks and valleys (Fig. 2, A and B). Moreover, the attractor landscape of the p53 network of MCF7 cells in the absence of DNA damage exhibited one point attractor representing proliferation that was nearly identical to that of the normal cells, except for the activation state of cyclin G (fig. S2A and compare Table 4, 0_MCF7, with Table 1, 0_normal). This landscape indicated a stable state of cell cycle progression, which matched that observed in simulations with normal cells under the same conditions.

The landscape of the p53 network of MCF7 cells undergoes an attractor transition from one point attractor in the absence of DNA damage (Fig. 3A, Table 4, and fig. S2A) to one cyclic attractor in response to DNA damage (Fig. 3B, Table 5, and fig. S2B). Although attractor landscape analysis of MCF7 cells in the presence of DNA damage exhibited p53 pulsing dynamics similar to those of normal cells, some of the cyclic attractor states differed from those of normal cells because of the difference in state values (compare Table 5, 1_MCF7, with Table 1, 1_normal). These differences were due to the predefined and unchanging activity states of PTEN, p14ARF, and cyclin G in MCF7 cells. Similar to normal cells, caspase was not active, and thus, p53-mediated cell death was not activated and the cells exhibited cell cycle arrest similar to that observed

for normal cells. Our simulation results were consistent with the experimental data on MCF7 cells (*5*) and indicated that the activation state of the components of the p53 network can be incorporated into the analysis to reflect the specific genetic composition of a cell.

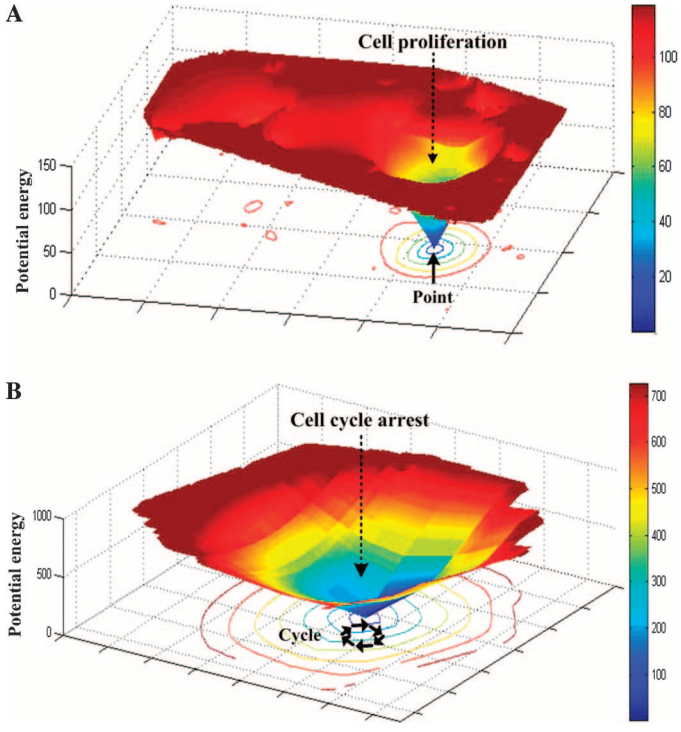

Fig. 3. Illustration of the potential energy landscape for the p53 regulatory network of MCF7 cells in the absence and presence of DNA damage. (**A**) Potential energy landscape for the p53 regulatory network of MCF7 cells in the absence of DNA damage. (**B**) The p53 network of MCF7 cells in the presence of DNA damage results in a cyclic attractor.

Identifying druggable targets and drug combinations to enhance p53-mediated apoptosis of MCF7 cells by attractor landscape analysis

From the single node and link deletion analysis of the normal cell p53 network, we identified critical nodes and links in the p53 network that could result in an apoptotic state when inhibited. We used this information to examine the efficacy of different inhibitory treatments for activating an apoptotic state in the p53 network of MCF7 cells using the attractor landscape framework. Several small molecules and peptides are already available that show antitumor activity by restoring or enhancing the tumor-suppressive activity of p53 (*35*–*38*).

The Mdm2-p53 link and the Wip1 node were selected for detailed investigation because these were critical for the induction of the cyclic attractor state associated with p53 oscillation (Fig. 2C). We did not select cyclin G because *cyclin G* is overexpressed in MCF7 cells (*33*), and it is likely that DNA damage would not trigger a sufficient reduction in cyclin G abundance to exert the deletion effect that we observed in the normal cells. Experimentally, the Mdm2-p53 interaction can be blocked by nutlin-3, a small-molecule inhibitor of Mdm2. Treatment of tumor cells with nutlin-3 increases the abundance of p53 and subsequently activates p53 target genes both in vitro and in vivo (*39*, *40*). Although nutlin-3 treatment results in nearly uniform cell cycle arrest at the G_1 and G_2 phases, apoptotic responses are variable (*39*, *41*). We simulated the response of MCF7 cells in which nutlin-3 treatment was represented by deletion of the Mdm2-p53 link in the absence of DNA damage and found that there were five point attractors, including two apoptotic point attractors defined as both p53 and caspase active (Table 4, 0_MCF7_nutlin-3). The attractor landscape of the p53 network of MCF7 cells with DNA damage and treated with nutlin-3 (lacking the Mdm2-p53 link) contained one large cyclic attractor and five point attractors (Table 5 and Fig. 4A). The basins of attraction for the cell death point attractors were relatively small, with basin sizes of 10,187 and 9127 in the absence of DNA damage, and 18,662 and 9284 in the presence of DNA damage (Tables 4 and 5). Because the basin size of an attractor indicates the number of all initial states that eventually reach the same attractor, these results suggested that nutlin-3 was not an efficient activator of cell death (the basin size can be considered as the probability of leading to a particular cell fate represented by the attractor). In addition, among the five point attractors, only two had activated caspase that would lead to cell death. Caspase was not active in the other three point attractors (Table 5). Instead, these had a persistent activation of p53. We defined persistent p53 activation without caspase activation as the cell fate of senescence, a permanent form of cell cycle arrest that is another attractive therapeutic target against cancer (*42*).

We performed a similar analysis of the p53 network in the presence and absence of DNA damage with Wip1 "inhibited" (the Wip1 node was deleted), which is another perturbation of the network predicted to induce cell death from the analysis of the normal cell p53 network (Table 2). In

Table 4. Stable states of the p53 network of MCF7 cells in the absence of DNA damage. Wip1 inhibition indicates that Wip1 was deleted from the network. Nutlin-3 inhibits the interaction between p53 and Mdm2. P, cell proliferation; A, cell cycle arrest; D, cell death; S, cell senescence.

DNA damage _condition	Type	ATM	p53	Mdm2	Mdmx	Wip1	cyclin G	PTEN	p21	AKT	cyclin E	Rb	E2F1	p14ARF	Bcl-2	Bax	caspase	Basin size (ratio)	Cell state
0_MCF7	Point			■			■			■	■		■		■			65,536 (1)	P
0_MCF7_nutlin-3	Point		■	■		■	■			■	■		■		■			45,925 (0.7008)	S
	Point		■	■		■	■		■	■			■			■	■	10,187 (0.1554)	D
	Point		■	■		■	■			■	■		■			■	■	9,127 (0.1393)	D
	Point		■	■		■	■		■	■			■		■			154 (0.0023)	S
	Point		■	■		■	■		■	■			■		■	■		143 (0.0022)	S
0_MCF7 Wip1 inhibition	Point			■			■			■	■		■		■			65,536 (1)	P
0_MCF7 _nutlin-3 _Wip1 inhibition	Point		■	■			■			■			■			■	■	29,120 (0.4443)	D
	Point		■	■			■			■	■		■		■			26,582 (0.4097)	S
	Point		■	■			■		■	■			■			■	■	9,267 (0.1414)	D
	Point		■	■			■			■	■		■		■			154 (0.0023)	S
	Point		■	■			■		■	■			■		■			143 (0.0022)	S

MCF7 cells without DNA damage, Wip1 removal resulted in one point attractor that corresponded to cell cycle progression (Table 4, 0_MCF7_Wip1 inhibition). In contrast, in the presence of DNA damage, removal of Wip1 from the p53 network of MCF7 cells produced a mixed pattern of cyclic and point attractors, of which two of the five point attractors represented cell death (Fig. 4B, Table 5, and fig. S4B). These attractors were similar to cellular states produced by nutlin-3 treatment; however, removal of Wip1 resulted in smaller basins of attraction for the cell death attractors than those produced by removal of the Mdm2-p53 link to represent nutlin-3 treatment. Although a previous study had shown that Wip1 inhibition in breast cancer cell lines with wild-type p53 induced cell death (*43*), our results predicted that such effect would be very small because the basin size of cell death attractors represented only ~5% of the entire attractor landscape. We observed that the greatest increase of total basin size of cell death point attractors occurred with the combinatorial treatment of nutlin-3 and Wip1 inhibition, irrespective of whether DNA damage is present (Fig. 4C, Table 5, and fig. S4C) or not (Table 4). In the presence of DNA damage in MCF7 cells, this combined treatment was predicted to induce ~71% of the cells to undergo cell death, compared to ~42% of cells undergoing death in response to nutlin-3 with DNA damage or ~4% of cells undergoing death in response to Wip1 inhibition with DNA damage (Table 5). Also, in the absence of DNA damage, this combinatorial treatment was predicted to induce ~58% of MCF7 cells to undergo cell death (Table 4).

Verifying the effectiveness of DNA damage combined with Wip1 inhibition and nutlin-3 in triggering cell death of MCF7 cells

To test the theoretical predictions from the attractor landscape analysis, we conducted single-cell imaging experiments to measure p53 dynamics and cell fate using a fluorescent MCF7 reporter cell line that stably expresses a wild-type p53-Venus construct (*5*). The dynamics of this p53-Venus construct have been studied in MCF7 cells, which confirmed that the reporter construct behaved similarly to endogenous p53 (*5*, *44*). We used a low dose of etoposide (10 μM) to induce DNA damage, which resulted in most cells entering cell cycle arrest (Fig. 5B). To inhibit Wip1 activity, we knocked down Wip1 by RNA interference (RNAi) (fig. S4). We quantified the p53 response to the different treatment conditions from the time-lapse movies by measuring the average yellow fluorescence in the nucleus (Fig. 5A and movies S1 to S5). Etoposide treatment alone and etoposide combined with Wip1 knockdown resulted in >85% of the MCF7 cells exhibiting p53 pulses, as reported previously for MCF7 cells exposed to γ-irradiation (*5*). Etoposide combined with nutlin-3 treatment produced a single p53 pulse in ~85% of the cells analyzed with the other 15% showing either multiple p53 oscillation or sustained p53, which is similar to the response of MCF7 cells to ultraviolet treatment (*45*). Nutlin-3 combined with Wip1 knockdown and triple treatment of etoposide with nutlin-3 and Wip1 knockdown produced a sustained increase in p53 activity in ~75% of the MCF7 cells, which was distinct from the p53 dynamics observed with the other treatments. We also determined the survival of the cells in response to the different treatments (Fig. 5B) and found that after 48 hours of treatment, cell death occurred with etoposide combined with nutlin-3 (~25% cell death), nutlin-3 combined with Wip1 knockdown (~90% death), and etoposide com-

Table 5. Stable states of the p53 network of MCF7 cells when DNA damage is induced.

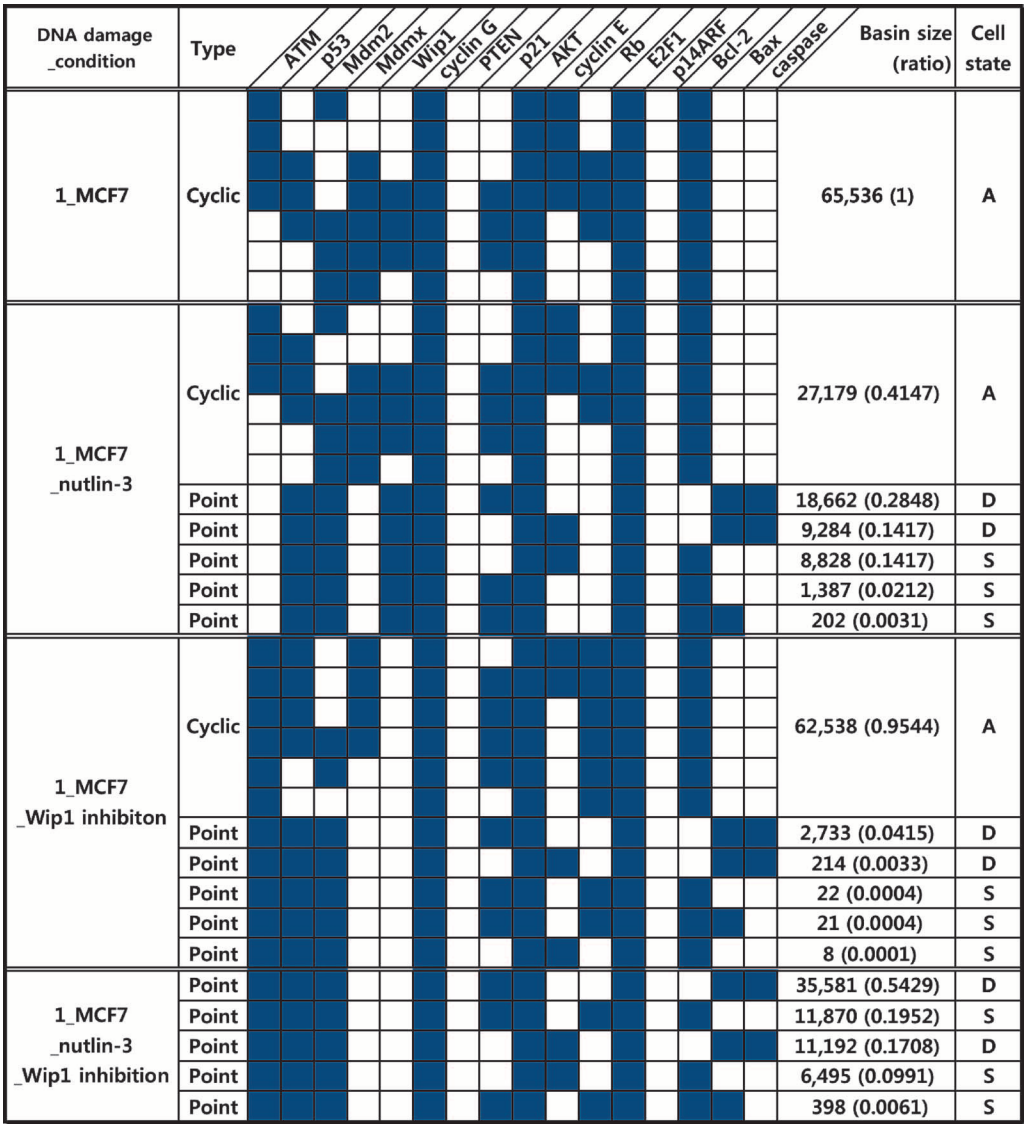

DNA damage _condition	Type	ATM	p53	Mdm2	Mdmx	Wip1	cyclin G	PTEN	p21	AKT	cyclin E	Rb	E2F1	p14ARF	Bcl-2	Bax	caspase	Basin size (ratio)	Cell state
1_MCF7	Cyclic	1	0	1	0	0	1	0	0	1	1	0	1	0	1	0	0	0	65,536 (1)	A
		1	0	0	0	0	1	0	0	1	1	0	1	0	1	0	0	0		
		1	0	0	1	0	1	0	0	1	1	1	1	0	1	0	0	0		
		1	0	0	1	0	1	0	1	1	1	1	1	0	1	0	0	0		
		0	1	1	1	0	1	0	1	0	1	1	1	0	1	0	0	0		
		0	0	1	1	0	1	0	1	0	0	1	1	0	1	0	0	0		
		0	0	1	1	0	1	0	1	0	0	1	1	0	1	0	0	0		
1_MCF7 _nutlin-3	Cyclic	1	0	1	0	0	1	0	0	1	1	0	1	0	1	0	0	0	27,179 (0.4147)	A
		1	1	0	0	0	1	0	0	1	1	0	1	0	1	0	0	0		
		1	1	0	1	1	1	0	0	1	1	1	1	0	1	0	0	0		
		0	1	1	1	1	1	0	1	0	1	1	1	0	1	0	0	0		
		0	0	1	1	1	1	0	1	0	0	1	1	0	1	0	0	0		
		0	0	1	1	0	1	0	1	0	0	1	1	0	1	0	0	0		
	Point	0	1	1	0	1	1	0	1	0	0	1	1	0	0	1	1	0	18,662 (0.2848)	D
	Point	0	1	1	0	1	1	0	0	1	0	1	1	0	0	1	1	0	9,284 (0.1417)	D
	Point	0	1	1	0	1	1	0	0	1	0	1	1	1	0	0	0	0	8,828 (0.1417)	S
	Point	0	1	1	0	1	1	0	1	1	0	1	1	1	0	0	0	0	1,387 (0.0212)	S
	Point	0	1	1	0	1	1	0	1	1	0	1	1	1	1	0	0	0	202 (0.0031)	S
1_MCF7 _Wip1 inhibiton	Cyclic	1	1	0	1	0	1	0	0	1	1	1	1	0	1	0	0	0	62,538 (0.9544)	A
		1	1	0	1	0	1	0	1	1	1	1	1	0	1	0	0	0		
		1	1	0	0	0	1	0	1	0	1	1	1	0	1	0	0	0		
		1	1	1	0	0	1	0	1	0	1	1	1	0	1	0	0	0		
		1	0	1	0	0	1	0	1	0	1	1	1	0	1	0	0	0		
		1	0	0	0	0	1	0	1	0	1	1	1	0	1	0	0	0		
	Point	1	1	1	0	0	1	0	1	0	0	1	1	0	0	1	1	0	2,733 (0.0415)	D
	Point	1	1	1	0	0	1	0	0	1	0	1	1	0	0	1	1	0	214 (0.0033)	D
	Point	1	1	1	0	0	1	0	1	0	1	1	1	0	1	0	0	0	22 (0.0004)	S
	Point	1	1	1	0	0	1	0	1	0	1	1	1	0	0	1	0	0	21 (0.0004)	S
	Point	1	1	1	0	0	1	0	0	1	1	1	1	0	1	0	0	0	8 (0.0001)	S
1_MCF7 _nutlin-3 _Wip1 inhibition	Point	1	1	1	0	0	1	0	1	0	0	1	1	0	0	1	1	0	35,581 (0.5429)	D
	Point	1	1	1	0	0	1	0	1	0	1	1	1	0	1	0	0	0	11,870 (0.1952)	S
	Point	1	1	1	0	0	1	0	0	1	0	1	1	0	0	1	1	0	11,192 (0.1708)	D
	Point	1	1	1	0	0	1	0	0	1	1	1	1	0	1	0	0	0	6,495 (0.0991)	S
	Point	1	1	1	0	0	1	0	1	0	1	1	1	0	0	1	0	0	398 (0.0061)	S

bined with nutlin-3 and Wip1 knockdown (~90% death). As predicted by the attractor landscape analysis, the degree of cell death correlated with the mode of p53 dynamics: Pulsing p53 generally resulted in cell cycle arrest and survival, whereas a sustained increase in p53 activity resulted in cell death (Fig. 5C). In addition, both the attractor landscape analysis and the experimental results showed that nutlin-3 combined with Wip1 knockdown can kill MCF7 cells even in the absence of DNA damage (Table 4 and Fig. 5B).

DISCUSSION

Our state-space analysis of the p53 regulatory network not only elucidated the differential p53 dynamics that modulate the cellular response to DNA damage but also showed that attractor landscape analysis can serve as a framework to explore druggable targets in a complex network. By constructing a Boolean model of the p53 network consisting of multiple feedback loops, we used state-space analysis with an attractor landscape to identify specific feedbacks that were critical for converting cyclic attractors to point attractors in response to DNA damage. We believe that this strategy enabled the characterization of p53 dynamics that modulate cell fate outcomes in response to DNA damage. Simulation results showed that p53 adopted the dynamic mode of either a series of discrete pulses or a sustained increase, which produced distinct cell fates under different conditions. The pulsing form of p53 activity, as revealed by the cyclic attractor, corresponded with cell cycle arrest, which would allow the cell time to repair the DNA damage (*4*, *46*). Our model suggested that when p53 was continuously activated, cell death would be effectively induced. The critical network structures identified by our analysis for the transition from a cyclic attractor to a point attractor provide insight for understanding the functional role of p53 dynamics in regulating cell fate.

Using the landscape framework, we examined and compared the efficacy of different anticancer strategies. We considered the size of the basins of the cell death attractor states produced by the different conditions as an indication of the efficacy of different treatments in inducing cell death. Our analysis showed that individual treatment with nutlin-3, which inhibits Mdm2-p53, or inhibition of Wip1 did not substantially enhance cell death in response to DNA damage because simulations of these conditions mainly produced a cyclic attractor consistent with oscillatory p53 dynamics and cell cycle arrest, instead of an attractor representing cell death. However, combinatorial treatment that simultaneously inhibited Wip1 and the Mdm2-p53 interaction resulted in a synergistic effect in producing large basins of cell death attractors, indicative of enhanced cell death, which was confirmed experimentally in MCF7 cells. Both our simulation and experimental results showed that treatment of nutlin-3 and inhibition of Wip1 can kill MCF7 cells even in the absence of DNA damage (Fig. 5B and Table 4). Thus, it appears that increasing p53 activity above a certain threshold is sufficient to trigger cell death, independent of the p53 post-translational modifications that are believed to rely on the DNA damage (*47*, *48*). Overall, our results suggest that combining nutlin-3 treatment with Wip1 inhibition and DNA-damaging agents may be a more effective therapeutic strategy to activate cancer cell death than nutlin-3 with DNA-damaging agents. Considering that MCF7 is a cell line that is resistant to the apoptotic effects of various anticancer treatments (*49*), our results may have important clinical implications. Moreover, the initial states of the p53 network could be different in different cells within the tumor, even for patients with the same type of cancer with the same genetic profile or among different patients. Our analysis suggested that this may lead to variable phenotypic responses to the same drug treatment because converging to any of the attractor states depended on the initial states of the network, even though the attractor landscapes were the same (fig. S2, C to E).

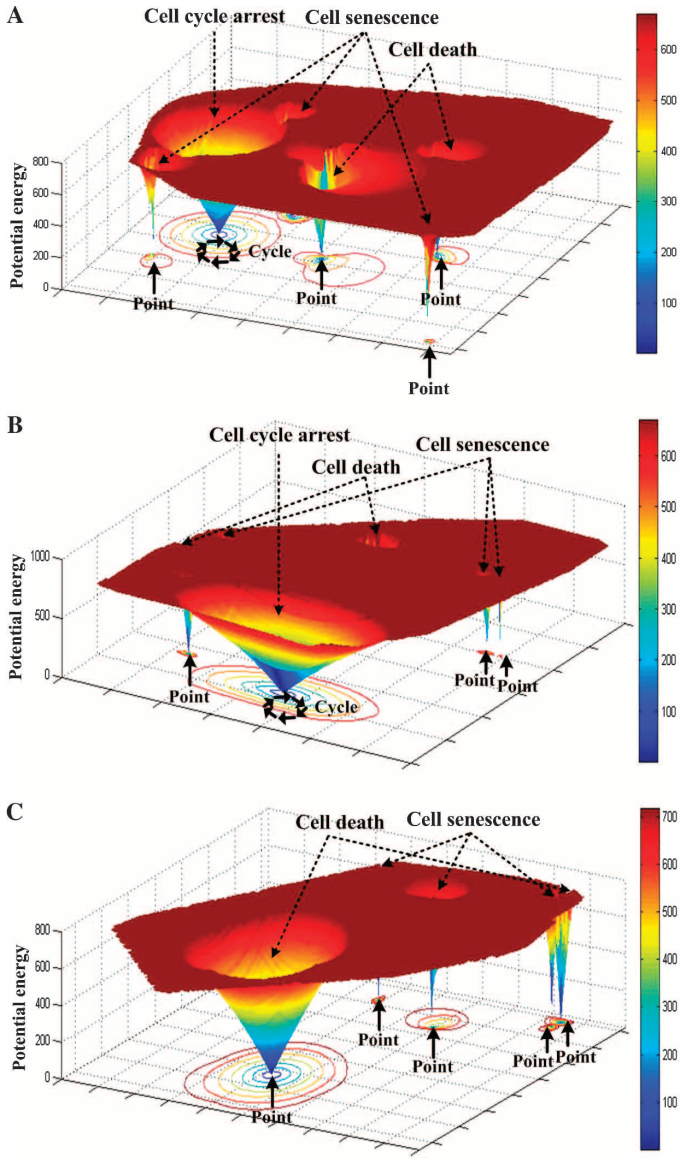

Fig. 4. Comparative analysis of the potential energy landscape of the p53 network of MCF7 cells after inhibitory treatments to induce cell death in the presence of DNA damage. (**A**) The potential energy landscape, reflecting the effect of nutlin-3 in MCF7 cells, consists of five point attractors and one cyclic attractor. (**B**) The potential energy landscape after deletion of the Wip1 from the network consists of five small basin point attractors and a large cyclic attractor basin. (**C**) The potential energy landscape after inhibition of the Wip1 in combination with treatment of nutlin-3 consists of five point attractors, with the largest basin representing the cell death state. See Table 5 for the sizes of the attractor basins.

The large basin of cell death attractor, such as that resulting from the combination of nutlin-3 treatment and Wip1 inhibition, may reduce such variability arising from the difference in initial states. From a therapeutic point of view, this combinatorial treatment may not only confer efficient cancer cell killing but also reduce the variable effects of drug treatment caused by individual variability.

Purvis *et al*. showed that change of p53 dynamics from pulsing to sustained increase would alter cell fate from transient cell cycle arrest to senescence (*29*), using detailed real-time quantitative polymerase chain reaction (qPCR) data for a set of p53 target genes, some of which are also network components in our model. Although the Boolean method that we used cannot provide time-series data as produced by the qPCR results, we can compare the gene expression characteristics and final gene expression [at the 24-hour time point shown in Fig. 2 of (*29*)] with our steady-state results. We found that our results regarding the regulation of CDKN1A (p21), Mdm2, Wip1, and Bax by the pulsing p53 (Table 5, 1_MCF7) agreed with those reported by Purvis *et al*.: CDKN1A, Mdm2, and Wip1 showed oscillatory responses in the presence of pulsing p53, whereas Bax was not induced. To generate a sustained p53 signal, Purvis *et al*. combined transient γ-irradiation with nutlin-3. This is similar to, but not exactly the same as, the continuous treatment of etoposide plus nutlin-3 in our study [Table 5 (1_MCF7_nutlin-3) and Fig. 5 (red curves)]. In response to etoposide combined with nutlin-3, we found that p53 dynamics in MCF7 cells changed from a series of short pulses to a long pulse. This long pulse in general lasts for ~20 hours, which is similar to the duration of the reported sustained p53 signal [shown in Fig. 1E of (*29*)]. Distinct from the study of Purvis *et al*., we found that p53 activity was prolonged even longer (the orange and purple curves in Fig. 5) by simultaneously inhibiting Mdm2 and Wip1, and such a sustained amount of p53 changed cell fate from cell cycle arrest to cell death. All of the previous studies on p53 dynamics and cell fate control only observed cell fate of either transient arrest or senescence, but not cell death. Considering that cell death may be a more desirable cancer treatment outcome than keeping the cells alive in the state of either transient arrest or senescence, our results could have important clinical implications for developing new anticancer regimens.

Although the classic epigenetic landscape proposed by Waddington is interpreted as a static surface (*50*), real biological systems must undergo transitions in the landscape when responding to various conditions, such as growth signals and DNA damage. Here, an attractor landscape of the p53 network was modeled for the relevant genotype of normal cells and cancer cells, in the absence or presence of DNA damage. Each attractor was assigned to a cellular phenotype on the basis of biological evidence.

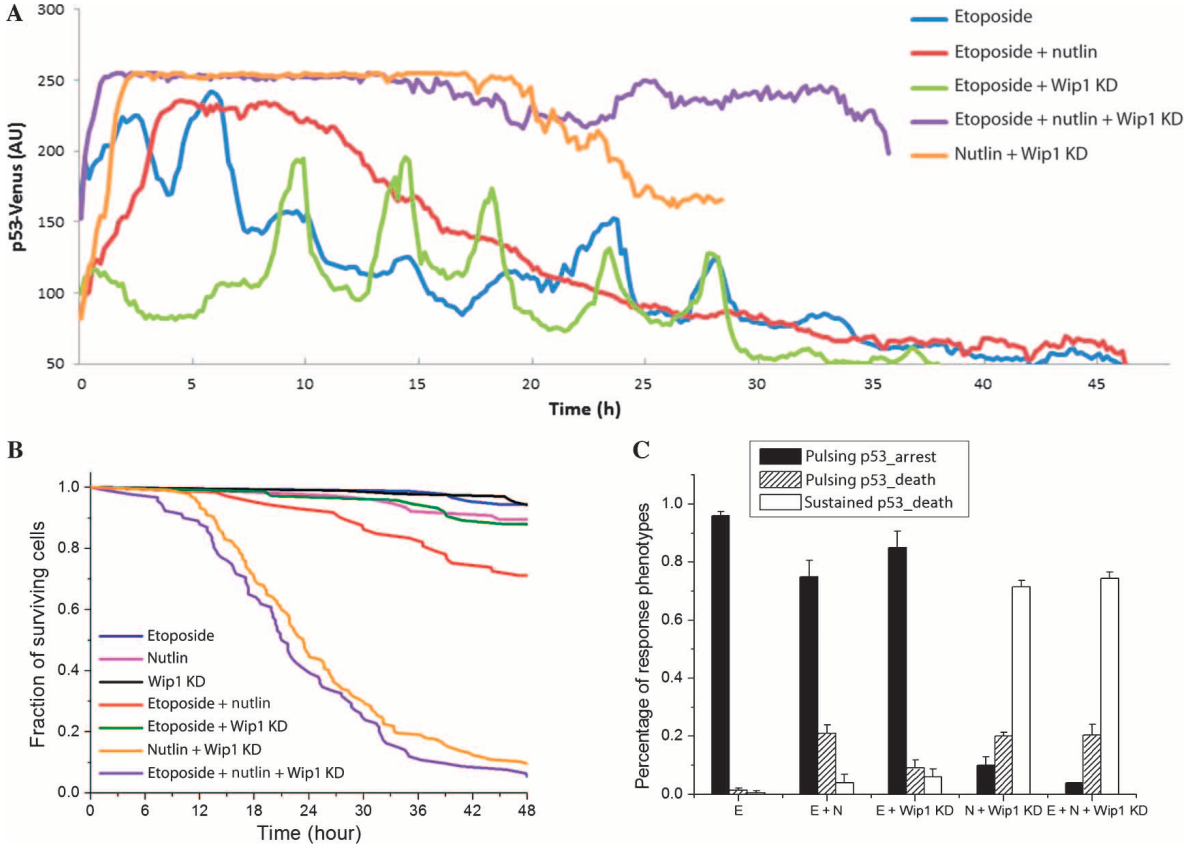

Fig. 5. Analysis of the effects of various treatments on p53 dynamics and cell fate in MCF7 cells. (**A**) Representative single-cell trajectories of p53 fluorescence in the nucleus under the following conditions: etoposide (10 μM), etoposide (10 μM) + nutlin-3 (10 μM), etoposide (10 μM) + Wip1 knockdown (KD), nutlin-3 (10 μM) + Wip1 KD, and etoposide (10 μM) + nutlin-3 (10 μM) + Wip1 KD. The abrupt end of p53 trajectory in the cells exposed to nutlin-3 + Wip1 KD and etoposide + nutlin-3 + Wip1 KD before 48 hours corresponds to cell death. AU, arbitrary units. (**B**) Cumulative survival curves for MCF7 cells with the indicated treatments. The total number of cells analyzed for each curve ranged from 73 to 105, varying between treatment conditions. Control siRNA was included in treatments of etoposide, nutlin-3, and etoposide + nutlin-3 to control for any pro-apoptotic effect of transfection. (**C**) Percentage of the three major cellular responses (phenotypes) to DNA damage: pulsing p53 followed by cell cycle arrest (denoted by filled black columns), pulsing p53 followed by cell death (lined columns), and sustained p53 followed by cell death (empty columns). Data were averaged from two separate sets of single-cell imaging experiments. E, etoposide; N, nutlin-3.

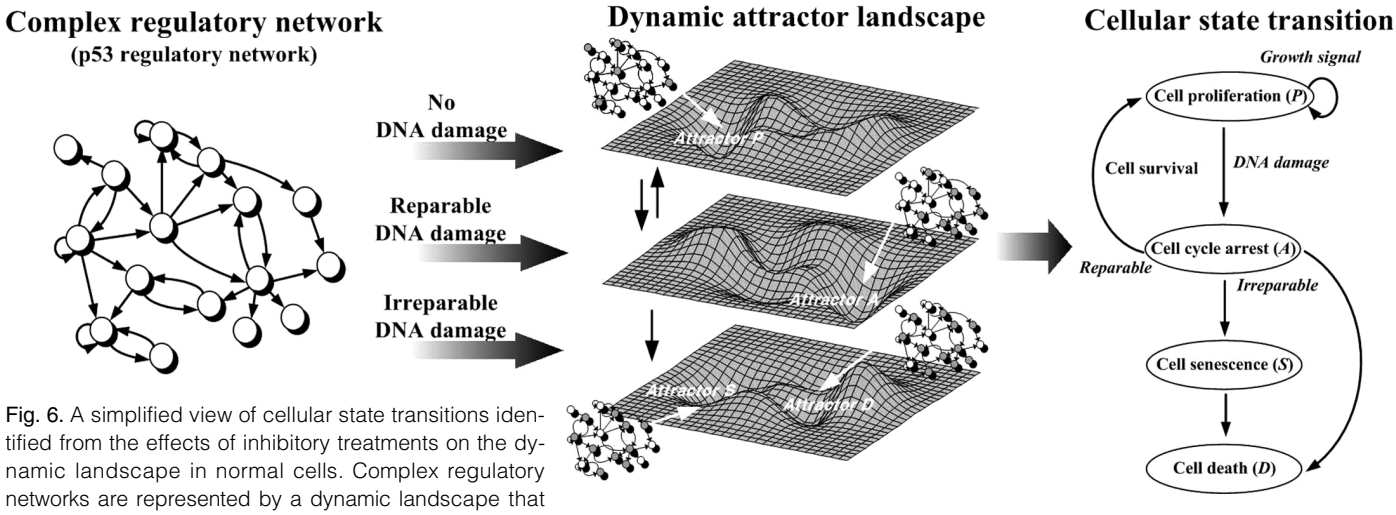

Fig. 6. A simplified view of cellular state transitions identified from the effects of inhibitory treatments on the dynamic landscape in normal cells. Complex regulatory networks are represented by a dynamic landscape that frequently changes its shape under various conditions. The cellular state can be assigned to one of four states: cell proliferation, cell cycle arrest, cell death, and cell senescence. Whereas cell fate is determined in the cell proliferation, cell death, and cell senescence states, each of which corresponding to a point attractor, it is not determined in the cell cycle arrest state, which is represented by a cyclic attractor. When DNA damage is induced in a normal cell, the cell cycle is arrested to allow damage repair. According to the reparability of the DNA damage, the cell selects its state among the determined states. Mutations can alter the cellular propensity to adopt particular cell states.

The shape of the attractor landscape changed in response to different conditions, and the changes included alterations in the stability of individual steady states and the appearance of novel steady states (Fig. 6). On the basis of these results, we divided the cell fate into four categories: proliferation, cell cycle arrest, death, and senescence. When the cell fate is cell survival (proliferation and senescence states) or cell death, it is uniquely determined from the point attractor. However, cell cycle arrest takes the form of a cyclic attractor and represents an intermediate cell fate, during which the decision to eventually enter into one of the uniquely determined fates is made, which we propose depends on the reparability of the DNA damage. In general, cancer cells are prevented from entering the death state and continue in the proliferation state, which are fundamental properties of cancer malignancy.

A delicate balance between proliferation and cell death is maintained in normal cells because of the presence of complex sensing mechanisms that activate the appropriate response (*45*, *51*). Our modeling analysis demonstrated that implementation of an attractor landscape to analyze a biological network is useful for acquiring a better understanding of the underlying complex network dynamics. As more quantitative, system-level data regarding the decision-making processes that govern cell fate become available, our approach could be used to construct more quantitative models adapted to specific cellular systems to predict the probability of a given cell adopting a particular cell fate, as a function of the stimuli. Additionally, this approach can be applied to reveal novel therapeutic strategies.

MATERIALS AND METHODS

A Boolean network model for the p53 network

We first constructed a simplified Boolean network model consisting of 16 nodes with multiple feedback loops through p53 for analyzing the p53 network. After building the simplified p53 regulatory network, we modeled the network dynamics using a deterministic Boolean network with a set of state transition logics defined on the basis of biological evidence. In the Boolean network model, each node is associated with a logic table that determines the output node for a given input (tables S4 and S5). Network dynamics were modeled by updating the Boolean functions, triggering system transits from the initial state to the final state, in which a network state is a collective binary representation of all variables. The state of each node can be either on (1) or off (0) at each time step. For computing the network dynamics, we transformed the state transition logic into a linear function. There are multiple sets of interaction weights and base levels for the linear function of each node that satisfy the same transition logic. Therefore, the interaction weights and base levels listed in table S4 are just one of the possible parameter sets. Among all the possible parameter sets for weights and base levels, we chose the minimal integer values for our study. We provided more details on the choice of parameters and described the range of possible parameter sets for each node that satisfy the same state transition logic in the Supplementary Materials [see supplementary text (section 2) and tables S4 and S5].

Potential energy landscape using transition probability

We first modeled the p53 network using deterministic Boolean network, with state transition logics that were based on experimental evidence. We then analyzed this network and identified all attractors and their basins. This deterministic model has, however, a limitation in that it cannot describe any uncertainty of cellular dynamic behavior that might be caused by intrinsic noise or extrinsic fluctuations. In a cell, statistical fluctuations coming from the finite number of molecules provide a source of intrinsic noise, and the fluctuations from dynamic and inhomogeneous environments of the exterior provide a source of external noise. Therefore, we extended the nominal deterministic Boolean network to a probabilistic Boolean network by introducing the state transition probability, based on Han and Wang's approach (*22*) that takes into account the uncertainties of biological systems. The reason why we opted for constructing the probabilistic network based on the deterministic Boolean network is as follows. If we model the p53 regulatory network using a probabilistic Boolean network without using a deterministic Boolean network, we need information about COD (coefficient of determination) to select a set of predictors for every node (*52*). Such COD information is difficult to acquire

from experiments, although not impossible, because experimental data are often incomplete. The alternative of considering all possible CODs for every node is also quite difficult because of the computational complexity. Using the extended probabilistic Boolean network, we calculated the steady-state probability distribution of each state and computed the potential energy landscape (supplementary text, section 3). Our results showed that each attractor of the deterministic Boolean network corresponds to the local energy minimum state in the potential energy landscape, and that the potential energy of the local minimum state is inversely proportional to the basin size of the attractor (see table S6 for details on the list of all states in the deterministic Boolean network together with the corresponding potential energy). A state space can be described by a directed graph where transitions among all 65,536 possible states are represented. For better intuitive conceptualization, each network state in the state-space plane can be assigned a potential energy, the height of which is inversely related to the probability that the network is found in that state, which in turn reflects its stability when the system is at equilibrium. The potential energy of each state in the attractor landscape is calculated from the steady-state probabilities by solving a discrete set of kinetic master equations for the network (*22*). The master equation for each state is defined as a time-varying probability, depending on the transition probabilities with respect to the neighboring states (see supplementary text, section 3). The state space was arranged into two-dimensional grids with minimal overlapping or crossing of the state connectivity. Each point on this two-dimensional grid represents a state (one of 65,536 states), but its *x*- and *y*-axis coordinate does not have a particular physical meaning. For the purpose of clear visualization, the state space was considered as *x* and *y* values in the attractor landscape with focus on the identification of attractor state.

Cell line, drug treatments, and RNAi

MCF7 cells were cultured under 37°C and 5% CO_2 in RPMI medium supplemented with 10% fetal calf serum (FCS), penicillin (100 U/ml), and streptomycin (100 μg/ml). To generate the fluorescent reporter cell line, we infected MCF7 cells with lentiviruses encoding an established p53-Venus reporter (*5*). The p53-Venus reporter construct, consisting of wild-type p53 fused to a yellow fluorescent protein, Venus, was a gift from G. Lahav at the Department of Systems Biology of Harvard Medical School. We selected an isogenic clone of the MCF7 p53 reporter cells that exhibited a dose response to etoposide most similar to that of the parental line. Etoposide and nutlin-3 were purchased from Sigma and Tocris, respectively. Small interfering RNA (siRNA) for knocking down Wip1 (UUGGCCUUGUGCCUACUAA) was custom-synthesized by Dharmacon. Dharmacon On-Target plus siControl (#D-001810-01) was used as nontargeting siRNA control. Both siRNAs were used at a final concentration of 20 nM, and siRNA transfections were performed with HiPerFect (Qiagen) according to the manufacturer's instructions. Experiments were conducted after 48 hours of gene silencing.

Single-cell imaging by time-lapse microscopy

MCF7 p53 reporter cells were plated in a 35-mm imaging dish (μ-dish, ibidi) and cultured in phenol red–free CO_2-independent medium (Invitrogen) supplemented with 10% FCS, penicillin (100 U/ml), and streptomycin (100 μl/ml). Cell images were acquired with a Nikon TE2000-PFS inverted microscope enclosed in a humidified chamber maintained at 37°C. Cells were imaged every 10 min for 48 hours, using a motorized stage and a 20× objective. Images were viewed and analyzed using the MetaMorph software (Molecular Dynamics). From phase-contrast images, we scored by morphological tracking the following cell states: interphase (by flat morphology), entry into mitosis (by cell rounding), cell division (by respreading and splitting), cell cycle arrest (by absence of cell division for 48 hours), and cell death (by blebbing followed by cell lysis). The dynamics of nuclear p53 was quantified on the basis of the p53-Venus fluorescence in the nucleus.

SUPPLEMENTARY MATERIALS

www.sciencesignaling.org/cgi/content/full/5/251/ra83/DC1
Text (sections 1 to 4)
Fig. S1. The attractor landscapes of the p53 regulatory network in normal cells under different conditions.
Fig. S2. The attractor landscapes of the p53 regulatory network in MCF7 cells in the absence and presence of DNA damage and with different inhibitory treatments.
Fig. S3. Robustness of the cyclic attractor against μ and *c*.
Fig. S4. Knockdown of Wip1 by RNAi in MCF7 cells.
Fig. S5. Transformation of a state transition logic into a linear function with the weight of each link and the base level (the basal activity) of each node.
Table S1. Positive and negative feedbacks interlinked through p53 in the p53 network.
Table S2. The stable states of the p53 network in response to each of the single node deletions.
Table S3. The stable states of the p53 network in response to each of the single link deletions.
Table S4. Boolean rules specifying the state transition logic.
Table S5. All the state transition logics and the range of possible parameter sets for each node that satisfy the same state transition logic.
Table S6. A list of all states in the deterministic Boolean network together with the corresponding potential energy in the probabilistic Boolean network.
References (*53*–*107*)
Movie S1. Supporting movie of p53 dynamics under etoposide alone.
Movie S2. Supporting movie of p53 dynamics under etoposide + nutlin-3.
Movie S3. Supporting movie of p53 dynamics under etoposide + Wip1 knockdown.
Movie S4. Supporting movie of p53 dynamics under etoposide + nutlin-3 + Wip1 knockdown.
Movie S5. Supporting movie of p53 dynamics under nutlin-3 + Wip1 knockdown.

REFERENCES AND NOTES

1. C. J. Bakkenist, M. B. Kastan, Initiating cellular stress responses. *Cell* **118**, 9–17 (2004).
2. D. W. Meek, Tumour suppression by p53: A role for the DNA damage response? *Nat. Rev. Cancer* **9**, 714–723 (2009).
3. J. T. Zilfou, S. W. Lowe, Tumor suppressive functions of p53. *Cold Spring Harb. Perspect. Biol.* **1**, a001883 (2009).
4. G. Lahav, Oscillations by the p53-Mdm2 feedback loop. *Adv. Exp. Med. Biol.* **641**, 28–38 (2008).
5. G. Lahav, N. Rosenfeld, A. Sigal, N. Geva-Zatorsky, A. J. Levine, M. B. Elowitz, U. Alon, Dynamics of the p53-Mdm2 feedback loop in individual cells. *Nat. Genet.* **36**, 147–150 (2004).
6. N. Geva-Zatorsky, N. Rosenfeld, S. Itzkovitz, R. Milo, A. Sigal, E. Dekel, T. Yarnitzky, Y. Liron, P. Polak, G. Lahav, U. Alon, Oscillations and variability in the p53 system. *Mol. Syst. Biol.* **2**, 2006.0033 (2006).
7. A. J. Levine, M. Oren, The first 30 years of p53: Growing ever more complex. *Nat. Rev. Cancer* **9**, 749–758 (2009).
8. A. J. Levine, W. Hu, Z. Feng, The p53 pathway: What questions remain to be explored? *Cell Death Differ.* **13**, 1027–1036 (2006).
9. Z. Mai, H. Liu, Boolean network-based analysis of the apoptosis network: Irreversible apoptosis and stable surviving. *J. Theor. Biol.* **259**, 760–769 (2009).
10. K. Puszyński, B. Hat, T. Lipniacki, Oscillations and bistability in the stochastic model of p53 regulation. *J. Theor. Biol.* **254**, 452–465 (2008).
11. C. J. Proctor, D. A. Gray, Explaining oscillations and variability in the p53-Mdm2 system. *BMC Syst. Biol.* **2**, 75 (2008).
12. R. V. Sionov, Y. Haupt, The cellular response to p53: The decision between life and death. *Oncogene* **18**, 6145–6157 (1999).
13. S. L. Harris, A. J. Levine, The p53 pathway: Positive and negative feedback loops. *Oncogene* **24**, 2899–2908 (2005).
14. S. Huang, G. Eichler, Y. Bar-Yam, D. E. Ingber, Cell fates as high-dimensional attractor states of a complex gene regulatory network. *Phys. Rev. Lett.* **94**, 128701 (2005).
15. S. Bhattacharya, Q. Zhang, M. E. Andersen, A deterministic map of Waddington's epigenetic landscape for cell fate specification. *BMC Syst. Biol.* **5**, 85 (2011).
16. S. Ding, W. Wang, Recipes and mechanisms of cellular reprogramming: A case study on budding yeast *Saccharomyces cerevisiae*. *BMC Syst. Biol.* **5**, 50 (2011).
17. J. M. Slack, Conrad Hal Waddington: The last Renaissance biologist? *Nat. Rev. Genet.* **3**, 889–895 (2002).

18. C. H. Waddington, The *Strategy of the Genes: A Discussion of Some Aspects of Theoretical Biology* (Allen & Unwin, London, 1957).
19. K. Vermeulen, D. R. Van Bockstaele, Z. N. Berneman, The cell cycle: A review of regulation, deregulation and therapeutic targets in cancer. *Cell Prolif.* **36**, 131–149 (2003).
20. K. Ohtani, J. DeGregori, J. R. Nevins, Regulation of the cyclin E gene by transcription factor E2F1. *Proc. Natl. Acad. Sci. U.S.A.* **92**, 12146–12150 (1995).
21. K. M. Boatright, G. S. Salvesen, Mechanisms of caspase activation. *Curr. Opin. Cell Biol.* **15**, 725–731 (2003).
22. B. Han, J. Wang, Quantifying robustness and dissipation cost of yeast cell cycle network: The funneled energy landscape perspectives. *Biophys. J.* **92**, 3755–3763 (2007).
23. Y. K. Kwon, K. H. Cho, Analysis of feedback loops and robustness in network evolution based on Boolean models. *BMC Bioinformatics* **8**, 430 (2007).
24. Y. K. Kwon, K. H. Cho, Coherent coupling of feedback loops: A design principle of cell signaling networks. *Bioinformatics* **24**, 1926–1932 (2008).
25. Y. K. Kwon, K. H. Cho, Boolean dynamics of biological networks with multiple coupled feedback loops. *Biophys. J.* **92**, 2975–2981 (2007).
26. D. A. Hamstra, M. S. Bhojani, L. B. Griffin, B. Laxman, B. D. Ross, A. Rehemtulla, Real-time evaluation of p53 oscillatory behavior in vivo using bioluminescent imaging. *Cancer Res.* **66**, 7482–7489 (2006).
27. A. Mirza, Q. Wu, L. Wang, T. McClanahan, W. R. Bishop, F. Gheyas, W. Ding, B. Hutchins, T. Hockenberry, P. Kirschmeier, J. R. Greene, S. Liu, Global transcriptional program of p53 target genes during the process of apoptosis and cell cycle progression. *Oncogene* **22**, 3645–3654 (2003).
28. X. P. Zhang, F. Liu, Z. Cheng, W. Wang, Cell fate decision mediated by p53 pulses. *Proc. Natl. Acad. Sci. U.S.A.* **106**, 12245–12250 (2009).
29. J. E. Purvis, K. W. Karhohs, C. Mock, E. Batchelor, A. Loewer, G. Lahav, p53 dynamics control cell fate. *Science* **336**, 1440–1444 (2012).
30. E. S. Helton, X. Chen, p53 modulation of the DNA damage response. *J. Cell. Biochem.* **100**, 883–896 (2007).
31. X. Zhang, G. Wan, S. Mlotshwa, V. Vance, F. G. Berger, H. Chen, X. Lu, Oncogenic Wip1 phosphatase is inhibited by miR-16 in the DNA damage signaling pathway. *Cancer Res.* **70**, 7176–7186 (2010).
32. X. Lu, O. Ma, T. A. Nguyen, S. N. Jones, M. Oren, L. A. Donehower, The Wip1 phosphatase acts as a gatekeeper in the p53-Mdm2 autoregulatory loop. *Cancer Cell* **12**, 342–354 (2007).
33. C. L. Reimer, A. M. Borras, S. K. Kurdistani, J. R. Garreau, M. Chung, S. A. Aaronson, S. W. Lee, Altered regulation of cyclin G in human breast cancer and its specific localization at replication foci in response to DNA damage in p53+/+ cells. *J. Biol. Chem.* **274**, 11022–11029 (1999).
34. Y. Liang, C. Yan, N. F. Schor, Apoptosis in the absence of caspase 3. *Oncogene* **20**, 6570–6578 (2001).
35. S. Shangary, S. Wang, Targeting the MDM2-p53 interaction for cancer therapy. *Clin. Cancer Res.* **14**, 5318–5324 (2008).
36. E. A. Bassett, W. Wang, F. Rastinejad, W. S. El-Deiry, Structural and functional basis for therapeutic modulation of p53 signaling. *Clin. Cancer Res.* **14**, 6376–6386 (2008).
37. C. R. Berkers, H. Ovaa, Drug discovery and assay development in the ubiquitin-proteasome system. *Biochem. Soc. Trans.* **38**, 14–20 (2010).
38. T. R. Hupp, D. P. Lane, K. L. Ball, Strategies for manipulating the p53 pathway in the treatment of human cancer. *Biochem. J.* **352** (Pt. 1), 1–17 (2000).
39. L. T. Vassilev, B. T. Vu, B. Graves, D. Carvajal, F. Podlaski, Z. Filipovic, N. Kong, U. Kammlott, C. Lukacs, C. Klein, N. Fotouhi, E. A. Liu, In vivo activation of the p53 pathway by small-molecule antagonists of MDM2. *Science* **303**, 844–848 (2004).
40. T. Van Maerken, L. Ferdinande, J. Taildeman, I. Lambertz, N. Yigit, L. Vercruysse, A. Rihani, M. Michaelis, J. Cinatl Jr., C. A. Cuvelier, J. C. Marine, A. De Paepe, M. Bracke, F. Speleman, J. Vandesompele, Antitumor activity of the selective MDM2 antagonist nutlin-3 against chemoresistant neuroblastoma with wild-type p53. *J. Natl. Cancer Inst.* **101**, 1562–1574 (2009).
41. C. Tovar, J. Rosinski, Z. Filipovic, B. Higgins, K. Kolinsky, H. Hilton, X. Zhao, B. T. Vu, W. Qing, K. Packman, O. Myklebost, D. C. Heimbrook, L. T. Vassilev, Small-molecule MDM2 antagonists reveal aberrant p53 signaling in cancer: Implications for therapy. *Proc. Natl. Acad. Sci. U.S.A.* **103**, 1888–1893 (2006).
42. I. B. Roninson, Tumor cell senescence in cancer treatment. *Cancer Res.* **63**, 2705–2715 (2003).
43. J. Pärssinen, E. L. Alarmo, R. Karhu, A. Kallioniemi, *PPM1D* silencing by RNA interference inhibits proliferation and induces apoptosis in breast cancer cell lines with wild-type p53. *Cancer Genet. Cytogenet.* **182**, 33–39 (2008).
44. E. Batchelor, C. S. Mock, I. Bhan, A. Loewer, G. Lahav, Recurrent initiation: A mechanism for triggering p53 pulses in response to DNA damage. *Mol. Cell* **30**, 277–289 (2008).
45. E. Batchelor, A. Loewer, C. Mock, G. Lahav, Stimulus-dependent dynamics of p53 in single cells. *Mol. Syst. Biol.* **7**, 488 (2011).
46. G. Lahav, The strength of indecisiveness: Oscillatory behavior for better cell fate determination. *Sci. STKE* **2004**, pe55 (2004).
47. N. D. Lakin, S. P. Jackson, Regulation of p53 in response to DNA damage. *Oncogene* **18**, 7644–7655 (1999).
48. M. B. Kastan, O. Onyekwere, D. Sidransky, B. Vogelstein, R. W. Craig, Participation of p53 protein in the cellular response to DNA damage. *Cancer Res.* **51**, 6304–6311 (1991).
49. E. Devarajan, J. Chen, A. S. Multani, S. Pathak, A. A. Sahin, K. Mehta, Human breast cancer MCF-7 cell line contains inherently drug-resistant subclones with distinct genotypic and phenotypic features. *Int. J. Oncol.* **20**, 913–920 (2002).
50. S. Huang, I. Ernberg, S. Kauffman, Cancer attractors: A systems view of tumors from a gene network dynamics and developmental perspective. *Semin. Cell Dev. Biol.* **20**, 869–876 (2009).
51. C. J. Bakkenist, M. B. Kastan, DNA damage activates ATM through intermolecular autophosphorylation and dimer dissociation. *Nature* **421**, 499–506 (2003).
52. I. Shmulevich, E. R. Dougherty, S. Kim, W. Zhang, Probabilistic Boolean networks: A rule-based uncertainty model for gene regulatory networks. *Bioinformatics* **18**, 261–274 (2002).
53. M. B. Kastan, J. Bartek, Cell-cycle checkpoints and cancer. *Nature* **432**, 316–323 (2004).
54. A. Ho, S. F. Dowdy, Regulation of G_1 cell-cycle progression by oncogenes and tumor suppressor genes. *Curr. Opin. Genet. Dev.* **12**, 47–52 (2002).
55. M. Arellano, S. Moreno, Regulation of CDK/cyclin complexes during the cell cycle. *Int. J. Biochem. Cell Biol.* **29**, 559–573 (1997).
56. R. A. Weinberg, The retinoblastoma protein and cell cycle control. *Cell* **81**, 323–330 (1995).
57. J. R. Nevins, The Rb/E2F pathway and cancer. *Hum. Mol. Genet.* **10**, 699–703 (2001).
58. O. Kranenburg, A. J. van der Eb, A. Zantema, Cyclin-dependent kinases and pRb: Regulators of the proliferation-differentiation switch. *FEBS Lett.* **367**, 103–106 (1995).
59. M. B. Kastan, D. S. Lim, The many substrates and functions of ATM. *Nat. Rev. Mol. Cell Biol.* **1**, 179–186 (2000).
60. E. U. Kurz, S. P. Lees-Miller, DNA damage-induced activation of ATM and ATM-dependent signaling pathways. *DNA Repair* **3**, 889–900 (2004).
61. K. S. Yee, K. H. Vousden, Complicating the complexity of p53. *Carcinogenesis* **26**, 1317–1322 (2005).
62. J. Pawlowski, A. S. Kraft, Bax-induced apoptotic cell death. *Proc. Natl. Acad. Sci. U.S.A.* **97**, 529–531 (2000).
63. D. T. Chao, S. J. Korsmeyer, BCL-2 family: Regulators of cell death. *Annu. Rev. Immunol.* **16**, 395–419 (1998).
64. J. S. Fridman, S. W. Lowe, Control of apoptosis by p53. *Oncogene* **22**, 9030–9040 (2003).
65. M. Fussenegger, J. E. Bailey, J. Varner, A mathematical model of caspase function in apoptosis. *Nat. Biotechnol.* **18**, 768–774 (2000).
66. Z. Zhang, H. Wang, M. Li, S. Agrawal, X. Chen, R. Zhang, MDM2 is a negative regulator of $p21^{WAF1/CIP1}$, independent of p53. *J. Biol. Chem.* **279**, 16000–16006 (2004).
67. Y. Jin, H. Lee, S. X. Zeng, M. S. Dai, H. Lu, MDM2 promotes $p21^{waf1/cip1}$ proteasomal turnover independently of ubiquitylation. *EMBO. J.* **22**, 6365–6377 (2003).
68. J. G. Kemeny, J. L. Snell, *Finite Markov Chains* (Springer-Verlag, New York, 1976).
69. J. J. Hopfield, Neural networks and physical systems with emergent collective computational abilities. *Proc. Natl. Acad. Sci. U.S.A.* **79**, 2554–2558 (1982).
70. M. Aldana, E. Balleza, S. Kauffman, O. Resendiz, Robustness and evolvability in genetic regulatory networks. *J. Theor. Biol.* **245**, 433–448 (2007).
71. X. Lu, B. Nannenga, L. A. Donehower, PPM1D dephosphorylates Chk1 and p53 and abrogates cell cycle checkpoints. *Genes Dev.* **19**, 1162–1174 (2005).
72. T. Ohtsuka, M. R. Jensen, H. G. Kim, K. T. Kim, S. W. Lee, The negative role of cyclin G in ATM-dependent p53 activation. *Oncogene* **23**, 5405–5408 (2004).
73. A. A. Goodarzi, J. C. Jonnalagadda, P. Douglas, D. Young, R. Ye, G. B. Moorhead, S. P. Lees-Miller, K. K. Khanna, Autophosphorylation of ataxia-telangiectasia mutated is regulated by protein phosphatase 2A. *EMBO J.* **23**, 4451–4461 (2004).
74. E. Berkovich, D. Ginsberg, ATM is a target for positive regulation by E2F-1. *Oncogene* **22**, 161–167 (2003).
75. E. Appella, C. W. Anderson, Post-translational modifications and activation of p53 by genotoxic stresses. *Eur. J. Biochem.* **268**, 2764–2772 (2001).
76. Q. Cheng, J. Chen, Mechanism of p53 stabilization by ATM after DNA damage. *Cell Cycle* **9**, 472–478 (2010).
77. T. M. Gottlieb, J. F. Leal, R. Seger, Y. Taya, M. Oren, Cross-talk between Akt, p53 and Mdm2: Possible implications for the regulation of apoptosis. *Oncogene* **21**, 1299–1303 (2002).
78. S. W. Lowe, C. J. Sherr, Tumor suppression by *Ink4a–Arf*: Progress and puzzles. *Curr. Opin. Genet. Dev.* **13**, 77–83 (2003).
79. H. Kawai, V. Lopez-Pajares, M. M. Kim, D. Wiederschain, Z. M. Yuan, RING domain–mediated interaction is a requirement for MDM2's E3 ligase activity. *Cancer Res.* **67**, 6026–6030 (2007).

80. X. Wu, J. H. Bayle, D. Olson, A. J. Levine, The p53–mdm-2 autoregulatory feedback loop. *Genes Dev.* **7**, 1126–1132 (1993).
81. L. Yamasaki, Role of the RB tumor suppressor in cancer. *Cancer Treat. Res.* **115**, 209–239 (2003).
82. X. Lu, T. A. Nguyen, S. H. Moon, Y. Darlington, M. Sommer, L. A. Donehower, The type 2C phosphatase Wip1: An oncogenic regulator of tumor suppressor and DNA damage response pathways. *Cancer Metastasis Rev.* **27**, 123–135 (2008).
83. V. Lopez-Pajares, M. M. Kim, Z. M. Yuan, Phosphorylation of MDMX mediated by Akt leads to stabilization and induces 14-3-3 binding. *J. Biol. Chem.* **283**, 13707–13713 (2008).
84. M. W. Jackson, M. S. Lindstrom, S. J. Berberich, MdmX binding to ARF affects Mdm2 protein stability and p53 transactivation. *J. Biol. Chem.* **276**, 25336–25341 (2001).
85. Y. Pan, J. Chen, MDM2 promotes ubiquitination and degradation of MDMX. *Mol. Cell. Biol.* **23**, 5113–5121 (2003).
86. X. Zhang, L. Lin, H. Guo, J. Yang, S. N. Jones, A. Jochemsen, X. Lu, Phosphorylation and degradation of MdmX is inhibited by Wip1 phosphatase in the DNA damage response. *Cancer Res.* **69**, 7960–7968 (2009).
87. M. Takekawa, M. Adachi, A. Nakahata, I. Nakayama, F. Itoh, H. Tsukuda, Y. Taya, K. Imai, p53-inducible Wip1 phosphatase mediates a negative feedback regulation of p38 MAPK-p53 signaling in response to UV radiation. *EMBO J.* **19**, 6517–6526 (2000).
88. S. Bates, S. Rowan, K. H. Vousden, Characterisation of human cyclin G1 and G2: DNA damage inducible genes. *Oncogene* **13**, 1103–1109 (1996).
89. V. Stambolic, D. MacPherson, D. Sas, Y. Lin, B. Snow, Y. Jang, S. Benchimol, T. W. Mak, Regulation of PTEN transcription by p53. *Mol. Cell* **8**, 317–325 (2001).
90. Y. Li, D. Dowbenko, L. A. Lasky, AKT/PKB phosphorylation of $p21^{Cip/WAF1}$ enhances protein stability of $p21^{Cip/WAF1}$ and promotes cell survival. *J. Biol. Chem.* **277**, 11352–11361 (2002).
91. A. L. Gartel, S. K. Radhakrishnan, Lost in transcription: p21 repression, mechanisms, and consequences. *Cancer Res.* **65**, 3980–3985 (2005).
92. I. Vivanco, C. L. Sawyers, The phosphatidylinositol 3-kinase–AKT pathway in human cancer. *Nat. Rev. Cancer* **2**, 489–501 (2002).
93. S. Polager, D. Ginsberg, E2F—At the crossroads of life and death. *Trends Cell Biol.* **18**, 528–535 (2008).
94. X. Tan, S. J. Martin, D. R. Green, J. Y. Wang, Degradation of retinoblastoma protein in tumor necrosis factor- and CD95-induced cell death. *J. Biol. Chem.* **272**, 9613–9616 (1997).
95. D. B. Yap, J. K. Hsieh, F. S. Chan, X. Lu, mdm2: A bridge over the two tumour suppressors, p53 and Rb. *Oncogene* **18**, 7681–7689 (1999).
96. J. T. Powers, S. Hong, C. N. Mayhew, P. M. Rogers, E. S. Knudsen, D. G. Johnson, E2F1 uses the ATM signaling pathway to induce p53 and Chk2 phosphorylation and apoptosis. *Mol. Cancer Res.* **2**, 203–214 (2004).
97. Z. Zhang, H. Wang, M. Li, E. R. Rayburn, S. Agrawal, R. Zhang, Stabilization of E2F1 protein by MDM2 through the E2F1 ubiquitination pathway. *Oncogene* **24**, 7238–7247 (2005).
98. D. Markham, S. Munro, J. Soloway, D. P. O'Connor, N. B. La Thangue, DNA-damage-responsive acetylation of pRb regulates binding to E2F-1. *EMBO Rep.* **7**, 192–198 (2006).
99. J. W. Zhu, D. DeRyckere, F. X. Li, Y. Y. Wan, J. DeGregori, A role for E2F1 in the induction of ARF, p53, and apoptosis during thymic negative selection. *Cell Growth Differ.* **10**, 829–838 (1999).
100. T. Kinoshita, T. Yokota, K. Arai, A. Miyajima, Regulation of Bcl-2 expression by oncogenic Ras protein in hematopoietic cells. *Oncogene* **10**, 2207–2212 (1995).
101. S. Pugazhenthi, A. Nesterova, C. Sable, K. A. Heidenreich, L. M. Boxer, L. E. Heasley, J. E. Reusch, Akt/protein kinase B up-regulates Bcl-2 expression through cAMP-response element-binding protein. *J. Biol. Chem.* **275**, 10761–10766 (2000).
102. D. G. Kirsch, A. Doseff, B. N. Chau, D. S. Lim, N. C. de Souza-Pinto, R. Hansford, M. B. Kastan, Y. A. Lazebnik, J. M. Hardwick, Caspase-3-dependent cleavage of Bcl-2 promotes release of cytochrome c. *J. Biol. Chem.* **274**, 21155–21161 (1999).
103. B. Antonsson, F. Conti, A. Ciavatta, S. Montessuit, S. Lewis, I. Martinou, L. Bernasconi, A. Bernard, J. J. Mermod, G. Mazzei, K. Maundrell, F. Gambale, R. Sadoul, J. C. Martinou, Inhibition of Bax channel-forming activity by Bcl-2. *Science* **277**, 370–372 (1997).
104. D. M. Finucane, E. Bossy-Wetzel, N. J. Waterhouse, T. G. Cotter, D. R. Green, Bax-induced caspase activation and apoptosis via cytochrome c release from mitochondria is inhibitable by Bcl-xL. *J. Biol. Chem.* **274**, 2225–2233 (1999).
105. A. Brunet, A. Bonni, M. J. Zigmond, M. Z. Lin, P. Juo, L. S. Hu, M. J. Anderson, K. C. Arden, J. Blenis, M. E. Greenberg, Akt promotes cell survival by phosphorylating and inhibiting a Forkhead transcription factor. *Cell* **96**, 857–868 (1999).
106. D. Ginsberg, E2F1 pathways to apoptosis. *FEBS Lett.* **529**, 122–125 (2002).
107. D. Sohn, F. Essmann, K. Schulze-Osthoff, R. U. Jänicke, p21 blocks irradiation-induced apoptosis downstream of mitochondria by inhibition of cyclin-dependent kinase–mediated caspase-9 activation. *Cancer Res.* **66**, 11254–11262 (2006).

Acknowledgments: We thank G. Lahav (Department of Systems Biology, Harvard Medical School) for the p53-Venus reporter construct. We also thank S.-Y. Shin, D. Shin, D. Kim, J. Kim, and J. I. Joo (Laboratory for Systems Biology and Bio-Inspired Engineering, Department of Bio and Brain Engineering, KAIST) for their critical reading and valuable comments. **Funding:** This work was supported by the National Research Foundation of Korea (NRF) grants funded by the Korea Government, the Ministry of Education, Science and Technology (MEST) (2009-0086964 and 2010-0017662). S.H.J. was financially supported by Hansung University. **Author contributions:** K.-H.C. designed the project and supervised the research; M.C., S.H.J., and K.-H.C. performed the mathematical modeling and analysis; J.S. and X.C. performed the experiments; and M.C., J.S., and K.-H.C. wrote the manuscript. **Competing interests:** The authors declare that they have no competing interests. **Data and materials availability:** Data and materials are available upon request.

Submitted 2 July 2012
Accepted 31 October 2012
Final Publication 20 November 2012
10.1126/scisignal.2003363
Citation: M. Choi, J. Shi, S. H. Jung, X. Chen, K.-H. Cho, Attractor landscape analysis reveals feedback loops in the p53 network that control the cellular response to DNA damage. *Sci. Signal.* **5**, ra83 (2012).